Charge Detection Mass Spectrometry Reveals Conformational Heterogeneity in MegaDalton-Sized Monoclonal Antibody Aggregates

For Submission to: Journal of the American Chemical Society

Jacob S. Jordan[†], Conner C. Harper[†], Fan Zhang[‡], Esther Kofman[‡], Mandy Li[‡], Karthik Sathiyamoorthy[‡], Jan Paulo Zaragoza[‡], Laurence Fayadat-Dilman[‡], and Evan R. Williams^{†*}

†Department of Chemistry, University of California, Berkeley, California, 94720-1460 † Discovery Biologics, Protein Sciences, Merck & Co., Inc., 213 E Grand Ave., South San Francisco, CA 94080, USA

*To whom correspondence should be addressed

e-mail: erw@berkeley.edu

Abstract

Aggregation of protein-based therapeutics can occur during development, production, or storage and can lead to loss of efficacy and potential toxicity. Native mass spectrometry of a covalently linked pentameric monoclonal antibody complex with a mass of ~800 kDa reveals several distinct conformations, smaller complexes, and abundant higher-order aggregates of the pentameric species. Charge detection mass spectrometry (CDMS) reveals individual oligomers up to the pentamer mAb trimer (15 individual mAb molecules; ~2.4 MDa) whereas intermediate aggregates composed of 6-9 mAb molecules and aggregates larger than the pentameric dimer (1.6 MDa) were not detected/resolved by standard mass spectrometry, size exclusion chromatography (SEC), capillary electrophoresis (CE-SDS), or by mass photometry. Conventional QTOF MS, mass photometry, SEC, and CE-SDS did not resolve partially or more fully unfolded conformations of each oligomer that were readily identified using CDMS by their significantly higher extent of charging. Trends in the charge-state distributions of individual oligomers provides detailed insight into how the structures of compact and elongated mAb aggregates change as a function of aggregate size. These results demonstrate the advantages of CDMS for obtaining accurate masses and information about the conformations of large antibody aggregates despite extensive overlapping m/z values. These results open up the ability to investigate structural changes that occur in small, soluble oligomers during the earliest stages of aggregation for antibodies or other proteins.

Introduction

Protein aggregation is a common factor in many devastating human diseases, including Alzheimer's disease, Parkinson's disease, and Huntington's disease among many others. 1,2 Many protein therapeutics are also prone to aggregation, which can degrade their efficacy and may lead to adverse patient outcomes. 3–5 Understanding factors that affect protein aggregation are important for the development, storage, and shipment of biopharmaceuticals. The effects of thermal and freeze/thaw stress on the aggregation of biotherapeutics are routinely characterized for FDA approval of new pharmaceuticals. 6 Characterization is typically done using methods such as optical, fluorescence, or electron microscopy, size-exclusion chromatography, capillary electrophoresis, and dynamic or multi-angle light scattering. 7 While these methods can often quantify changes in the abundances of higher order, visible aggregates or protein monomers and dimers, the resolution at intermediate aggregate sizes (>10 nm - <100 nm) may be limited so that individual oligomeric states are not distinguished.

Native mass spectrometry (MS) is routinely used for characterizing proteins, DNA, and the stoichiometry and structures of macromolecular complexes owing to the inherent high sensitivity and speed of analysis. Native MS has been extensively used to characterize the masses, stoichiometries, and stabilities of monoclonal antibody therapeutics (mAbs) and drugantibody complexes.^{8–11} However, characterizing higher order aggregates with conventional MS instruments can be challenging because of detection and resolution limitations associated with high *m/z* measurements and the heterogeneity of large molecular complexes. Heterogeneity can be intrinsic to the sample itself, but also can be the result of adduction of non-volatile salts, molecules, and solvent to gaseous ions that are formed directly from solution by electrospray ionization.^{12,13} Adducts broaden peaks in a charge-state distribution, an effect that can ultimately

prevent individual charge states from being resolved. Under these circumstances, little information about masses is obtained directly from a mass spectrum. The extent of heterogeneity typically increases with analyte mass, but limitations on resolving power as a result of sample heterogeneity are sample dependent. The lack of a robust method for measuring the masses and stoichiometries of higher molecular weight analytes using conventional MS instrumentation often precludes the characterization of the distribution of higher order oligomers for many biomolecules of pharmaceutical interest, especially when analyte masses extend into the MDa range.

Charge detection mass spectrometry (CDMS), in which the m/z and charge of individual ions are measured independently, overcomes the high mass limitations of conventional MS instruments. CDMS has been used to measure the masses of a diverse array of analytes, including intact viruses, ^{14–19} virus-like particles, ^{11,20,21} large protein complexes, ^{22,23} cellular replication and folding machinery, ^{24,25} synthetic polymers, ^{21,23,26–29} large salt clusters, ³⁰ aqueous nanodroplets, ^{31,32} and synthetic nanoparticles with masses extending into the high MDa and even GDa range.^{33–35} The advantage of individual ion measurements is that chemical noise is eliminated – the mass of each ion is measured independently of other ions. This makes it possible to obtain accurate masses for even highly heterogeneous analytes. 14,18 More recently, Orbitrap instruments have been used to make individual ion measurements as well.^{36–41} Mass measurements of individual large biomolecules can also be made with mass photometry, which relies upon the scattering of incident light as biomolecules interact with a glass surface, 42-44 and nanoelectromechanical sensor mass spectrometry, which measures the change in the resonant frequency of a nanofabricated sensor upon landing of a particle. 45–47 CDMS has been compared to mass photometry and size exclusion chromatography for the characterization of small, heavily

glycosylated antibody therapeutics⁴⁰ and recent differential ion mobility separations show this method can provide information about mAb oligomers as large as ~1.2 MDa.⁴⁸ CDMS has advantages for investigating antibody aggregation and aggregation-induced conformational changes, including the ability to measure molecular complexes with masses well into the 100's of MDa range. Here, we compare conventional native MS, mass photometry, size exclusion chromatography, capillary electrophoresis, and CDMS for characterizing the oligomeric distribution of a covalently bound complex consisting of five identical mAb molecules.⁴⁰

Experimental

A representative humanized IgG1 antibody heavy chain (HC) was designed with an appended, slightly modified human cartilage oligomeric matrix protein (COMP) motif (Uniprot: P49747, pos29-73, DLAPQMLRELQETNAALQDVRELLRQQVKEITFLKNTVMECDACG) following a (G₃S)₄ flexible linker at its C-terminus to promote pentameric assembly through disulfide and coiled-coil formation. This engineered HC and the corresponding kappa light chain (LC) were cloned separately for co-transfection into *in-house* mammalian expression vectors with signal peptides to promote secretion of the recombinant pentameric antibody. Plasmids for HC and LC were transiently transfected at 1:1 DNA ratio into a 293 cell expression system in suspension using serum-free defined media (Invitrogen Corporation, Carlsbad, CA). Cell culture supernatants were harvested after 4-days. High-throughput Protein-A based MabSelect affinity chromatography using miniature columns (Repligen/Cytiva, Waltham, MA) enabled 1-step purification of recombinant antibodies from the harvested clarified cell culture fluid (CCCF) to generate purified material.

Size exclusion chromatography (SEC) was performed using a Waters Acquity BEH450 column (2.5 μ m, 4.6 x 150 mm, Milford, MA) using an isocratic flow of 100 mM sodium phosphate, 200 mM sodium chloride, and 0.02% sodium azide (pH 7). Chromatograms were acquired using both 214 and 280 nm wavelengths, and integration of the absorption at 280 nm was performed using EMPOWER 3 (Waters Corporation). The molecular weights of unknowns were calculated based on the retention time of standards with known molecular weights between 112 Da and ~1.3 MDa analyzed using the same SEC conditions.

Capillary electrophoresis sodium dodecyl sulfate (CE-SDS) was done using a MauriceFlex instrument and CE-SDS PLUS cartridge (Bio-Techne, Minneapolis, MN) under non-reducing conditions. The CE-SDS PLUS molecular weight (MW) marker was supplemented with thyroglobulin to extend the range to 660 kDa. The sample was diluted in CE-SDS PLUS 1X sample buffer to make a 50 μL solution of 0.5 mg/mL protein. Iodoacetamide (IAA) was used as the alkylation reagent. 2 μL of CE-SDS PLUS 25X Internal Standard and 2.5 μL of 250 mM IAA were added to the sample and the sample was heated for 10 min at 70 °C. The MW marker and sample were run with injection at 4600 V over 20 s and separation at 5750 V for 90 min. Analysis of the acquired data was performed using the Compass for iCE software (Bio-Techne).

Mass photometry (MP) was performed using a Refeyn TwoMP instrument (Refeyn Ltd., Oxford, UK). Thyroglobulin and phosphate-buffered saline were used as a calibrant and as a blank, respectively. The sample was diluted in phosphate buffered saline (PBS) to a final concentration within an ideal working range of 10-50 nM. For data acquisition, 18 μ L of buffer was added to a well, followed by the addition of 2 μ L of the diluted sample. The well contents were mixed thoroughly, and measurements were started within a duration of 60 s. Analysis of the acquired data was performed using the DiscoverMP software (Refeyn Ltd.).

For mass spectrometry measurements, covalently linked pentameric mAb complexes were buffer exchanged into aqueous 163 mM ammonium acetate (pH 6.8) using a Micro Bio-Spin 6 column (Bio-Rad Laboratories, Hercules, CA). Ions were formed by electrospray (ESI) from borosilicate emitters that are pulled to a 1.1 ± 0.1 µm tip diameter. Emitters were fabricated in-house from borosilicate capillaries (1.0 mm outer diameter, 0.78 mm inner diameter, Sutter Instrument, Novato, CA, Part No. BF100-78-10) using a P-87 Flaming/Brown micropipette puller (Sutter Instrument).⁴⁹ Tip diameters were measured using a Hitachi TM-1000 scanning electron microscope (Tokyo, Japan) at the Electron Microscopy Laboratory at the University of California, Berkeley.

Data were acquired using a quadrupole time-of-flight (QTOF) Premier mass spectrometer (Waters Corporation, Milford, MA). The source temperature was 80 °C, and the extraction cone, sampling cone, and ion guide voltages were 3 V, 100 V, and 2 V, respectively. The backing pressure in the source was 5-10 mbar to assist desolvating larger ions. The collision gas flow rate was 0.75 mL min⁻¹, resulting in a final argon gas pressure of ~0.002 mbar in the collision cell. Ions were formed by applying a voltage of ~0.7 – 1.3 kV to a 0.127 mm platinum wire inserted into the back of nESI emitters and in contact with the solution.

Charge detection mass spectrometry experiments were performed using an instrument and data analysis methods that are described in detail elsewhere. 19,33,50 The instrument consists of a heated ion transfer tube maintained at 140 °C, three RF-only quadrupole ion guides, and an electrostatic cone trap. 33 To enable transmission over a wide range of m/z values ($m/z = \sim 2,000 - 20,000$), data were acquired by sweeping across five different tuning conditions by varying the voltages and frequencies of the RF-only quadrupoles and ion funnel. Reported relative abundances are based on the peak height (in counts) of each species. These data were analyzed

with a 10 ms short time Fourier transform window length. All mass spectrometry experiments were performed at the University of California, Berkeley. All other experiments were performed at Merck & Co., Inc., San Francisco, CA, USA.

Results and Discussion

QTOF MS and CDMS Characterization of the Pentamer mAb Sample

A covalent pentameric IgG1 complex (valency = 10) was produced through disulfide bond linkage and non-covalent interactions through a coiled-coil motif at the C-terminus of the heavy chain (HC) of a conventional mAb. This pentamer form could induce clustering of specific membrane receptors favoring functional downstream cell signaling pathways. An electrospray mass spectrum of the pentamer mAb complex acquired with a QTOF mass spectrometer shows a variety of highly charged species, including two elongated forms of the pentamer mAb with measured masses of $800.3 \pm 0.2 \text{ kDa}$ (m/z values between 4,000 and 5,500; charge states +140 - +185) and $800.7 \pm 0.4 \text{ kDa}$ (m/z values between 6,500 and 7,500; charge states +104 - +124), as well as a $400.1 \pm 0.1 \text{ kDa}$ ion (m/z values between 4,000 and 5,000; charge states +69 - +102) that does not correspond to a complex with an integer number of mAb molecules (Figure 1a). The extent of protein charging from electrospray ionization is related to the conformation or shape of proteins in solution. Higher charge ions are produced from proteins with more elongated conformations, indicating that the predominant species in the sample are elongated pentamer mAbs.

There are also many compact species observed in the QTOF mass spectrum, including a compact monomeric form of the pentamer mAb complex with a measured mass of 799.6 ± 0.8 kDa) (m/z values between 12,000 and 14,000; charge states between +57 and +67) (Figure 1a).

There is also signal for the mAb heavy chain (m/z = 3100 - 3600, 47.1 ± 0.1 kDa) and the mAb monomer (m/z = 5900 - 6500, 160.1 ± 0.1 kDa). Charge-state distributions between m/z 8,000 – 11,000 correspond to ions with masses of 320.7 ± 0.1 kDa, 488.1 ± 0.6 kDa, and 384.2 ± 0.2 kDa. The first two correspond to a dimer and trimer mAb complex, respectively, whereas the third may correspond to an aggregate or ion consisting of a mAb dimer and a heavy chain. The broad peaks and elevated baseline between m/z 3,000 and 11,000 clearly indicate the presence of other species that are unresolved. Although masses can be obtained for the dimer and trimer in this region, other components contributing to the signal underneath these distributions cannot be obtained directly.

There is a broad, unresolved peak at m/z = 16,000 - 19,000 (Figure 1a). Because charge-state resolution was not achieved, a mass was not obtained, but it almost certainly corresponds in part to a dimer of the pentamer complex (\sim 1.6 MDa) based on the m/z range. The pentamer appears to be relatively homogenous based on the resolved charge-state distributions, but salt or solvent adduction as well as binding of smaller species to high mass ions can lead to broad, overlapping peaks in a m/z spectrum that are not resolved, making it more difficult to characterize MDa-sized complexes. There is no identifiable signal for oligomers larger than the dimer of the pentamer complex.

The same pentamer sample was analyzed using CDMS and these data are shown in the form of a mass histogram (Figure 1b) and a two-dimensional representation of the same mass and charge data (Figure 1c). The mass histogram (Figure 1b) is analogous to a deconvolved mass spectrum obtained with conventional mass spectrometers. The two-dimensional plot (Figure 1c) provides information about the extent of charging or shape of the complexes. Both highly elongated and compact species are observed. The different structures can be distinguished based

on the differing number of charges even for ions that have the exact same mass. Highly elongated forms of the monomer ($161.1 \pm 0.5 \text{ kDa}$), dimer ($324.1 \pm 0.9 \text{ kDa}$), trimer ($478.8 \pm 1.2 \text{ kDa}$), tetramer ($647.1 \pm 2.0 \text{ kDa}$), and pentamer mAbs ($799.2 \pm 0.9 \text{ kDa}$) are abundant. There is also an ion at $402.8 \pm 2.6 \text{ kDa}$ that does not correspond to an integer number of mAbs that was also observed in the QTOF data. The masses determined from the highly charged forms of these species are in good agreement with the masses obtained from the QTOF mass spectra. There are also a number of highly charged oligomers consisting of the pentamer mAb and and smaller mAb oligomers. The largest oligomer is a highly charged form of the pentamer mAb trimer (15 mAbs, $2.40 \pm 0.01 \text{ MDa}$). Each of the high charge forms of these aggregates span a similar m/z range ($\sim 4,000 - 6,000$) and are likely present in the QTOF mass spectrum but are not resolved underneath the distribution for the abundant, elongated form of the pentamer. These data demonstrate that CDMS can quantify low abundance species when there are many ions of similar and overlapping m/z, making it possible to identify the composition of biotherapeutic samples that contain multiple species.

In addition to the high charge state forms of the complexes, lower charge distributions are also observed for each oligomer in the CDMS data, consistent with more compact conformations. The most abundant low charge species is the pentamer mAb (825.0 \pm 2.6 kDa) with an average charge of +64, similar to that in the QTOF data (+62). In the QTOF data, the higher charged forms of this complex are the most abundant form of the pentamer mAb whereas the more compact form is more abundant in the CDMS data. This difference in abundance may be due to lower ion transmission and/or lower detection efficiency of high m/z ions in the QTOF instrument. The compact dimer of the pentamer complex (1.61 \pm 0.01 MDa) consisting of a total of 10 mAb molecules is ~16% abundance relative to the compact monomer. Other low charge,

lower mass species are also observed, including the mAb monomer (173.1 \pm 5.2 kDa, at low abundance), dimer (344.4 \pm 5.1 kDa), trimer (492.7 \pm 5.1 kDa), and tetramer (657.1 \pm 4.3 kDa), as well as a 420.8 ± 12.1 kDa complex corresponding to a non-integer number of mAbs (Figure 1c). The CDMS masses for these compact species are ~2-8% higher than the masses obtained from the QTOF data and from the higher charge forms of these oligomers in the CDMS data. Higher protein charge states retain fewer adducts compared to lower charge states, 52-54 indicating that the overweight masses obtained for the compact forms of these oligomers is likely caused by adduction of small molecules, including water, as a result of the gentle conditions of the CDMS instrument. Additional activation of the ions prior to CDMS detection should reduce this mass discrepancy as is often done with conventional MS instruments. The mAb tetramer was not observed in the QTOF MS data, but the low abundance of this ion in CDMS data indicates that it may contribute to the heterogeneity between m/z = 10,000 - 11,000 in the QTOF mass spectrum. The abundance of the pentameric dimer is significantly higher in the CDMS data than in the QTOF data. CDMS indicates that the higher charged forms of the pentameric dimer are ~5.9 times greater in abundance than that of the lower, more compact form. These ions appear in a similar range of m/z as the elongated pentamer. These are not resolved in the QTOF data but would contribute to signal intensity attributed to the pentamer in this region. This same phenomenon of overlapping m/z distributions is true for other more extended forms of the large oligomers. Another contributing factor to differences in signal abundances between the QTOF and CDMS data at high mass is that there is not a detection mass bias in CDMS once the number of charges on an ion exceeds the detection limit, 33 but sensitivity decreases at high m/z in QTOF instruments. We conclude that the abundance of pentameric dimer measured in CDMS is more reflective of the solution composition.

Some aggregation can occur as a result of analyte concentration during electrospray droplet evaporation. 13,54 To determine if that is possible here, the average number of molecules per droplet was estimated from the droplet size formed from an emitter with a tip diameter of 1.1 μ m and \sim 1 μ M analyte concentration. $^{13,55-57}$ Under these conditions, there is on average one analyte molecule per twelve droplets, indicating that significant aggregation in the electrospray process is unlikely and that the oligomers must originate from solution. Because the m/z and z are determined independently with CDMS, it is possible to resolve a broad variety of species that have overlapping m/z values, but different extents of charging. As a result, CDMS shows significant promise as a technique for measuring the relative abundances of compact and elongated species with sufficient resolution to identify and characterize different forms of individual antibody oligomers.

Comparing MS-Based Characterization with Conventional Techniques

Aggregation in biopharmaceutical products is typically characterized using methods such as size exclusion chromatography (SEC), capillary electrophoresis sodium dodecyl sulfate (CE-SDS), and more recently, mass photometry. A mass photometry histogram was acquired on the same pentamer mAb sample (Figure 2a). There are peaks at 819 ± 32 kDa and 1.64 ± 0.06 MDa that correspond to the pentameric mAb complex and its dimer. The few counts between 2.3 MDa and 2.7 MDa may indicate the presence of a pentamer mAb trimer, but the mass spread in these data indicate that the signal is due to background noise or conformational heterogeneity of the higher order aggregates (Figure 2a). Mass photometry also indicates the presence of several lower mass species (80 ± 23 kDa, 326 ± 24 kDa and 485 ± 25 kDa) which may correspond to a mAb heavy chain, as well as two and three mAb complexes (Figure 2a). There is also a broad

peak centered at 1.29 ± 0.10 MDa that may correspond to aggregates of the pentamer mAb and other smaller mAb species (Figure 2a). The mass photometry data do not provide any indication of the different forms of the pentameric complex that are clearly distinguished in the mass spectrometry datasets.

The same pentamer mAb sample was analyzed using a standard SEC workflow for antibody analysis. The SEC data for the pentamer mAb sample has three predominant peaks at 3.00 min (621 kDa), 2.63 min (1.28 MDa), and 2.42 min (1.80 MDa) (Figure 2b). These masses do not correspond to any of the species observed by QTOF MS, CDMS, or by mass photometry. SEC separates analytes based on hydrodynamic radius, but samples containing multiple oligomers that each have conformational heterogeneity can result in ambiguous assignments of masses and identities to peaks in the SEC trace. Column interactions may also play a role in the ambiguous assignment of peak identities. Fractions were collected for each these three peaks and characterized using QTOF MS and CDMS. Both QTOF and CDMS mass spectra of the main peak fraction (2.63 min) show approximately equal abundances of the compact and elongated form of the pentamer mAb monomer as well as the smaller mAb dimer, trimer and a ~400 kDa species that does not correspond to an integer number of mAb monomers (Figure S1a,b). A low abundance of compact pentamer mAb dimer was also detected. No protein signal was resolved in fractions collected from other peaks in the SEC trace. These data indicate that standard SEC workflows for mAb characterization do not sufficiently separate the individual oligomeric forms of the pentamer mAb. While additional fraction collections with MS analysis and optimization of the SEC separations would likely lead to improved separation and information, a standard workflow for mAb characterization was chosen as being most representative of the information that is obtained from a standard analysis as was done for the other methods.

This sample was also characterized using nonreducing CE-SDS separations, which resulted in 8 peaks. The most abundant peak at 3.28 min likely corresponds to the pentamer mAb. The molecular weight determined by CE-SDS for the pentamer is 674 kDa, which is 15.8% lower than the mass determined by mass spectrometry. There are several sources of error in determining the molecular weight of proteins using CE-SDS, making identification of the other peaks ambiguous.⁵⁸ The presence of species both larger and smaller than the pentamer mAb is consistent with the data obtained by mass spectrometry and mass photometry. In contrast to these conventional methods, CDMS provides information about the mass and conformation of individual antibody oligomers from a single measurement, and these data make it possible to unambiguously identify species based on their mass and charge.

Characterizing the Conformational Heterogeneity of mAb Oligomers with CDMS

The ability to clearly resolve different conformations from the charge-state distribution of each oligomeric state of the mAb monomer can provide insight into how the structure of successive oligomers evolves with their increasing size. There are both compact and more elongated forms of all of the oligomers observed in the CDMS data. The charge-state distribution of the compact and elongated species for each oligomer are shown as a function of the number of mAb molecules in the oligomer in Figure 3. The abundances of both forms are normalized separately so that they can be more clearly seen on the combined plot. The average charge of the most compact structures (charged near the Rayleigh limit) gradually increases from $\sim 32~e$ to $\sim 95~e$ as the oligomer size increases from the n = 1 to n = 9, where n refers to the number of mAb molecules in the oligomer (Figure 3, compact conformations shown in red). The n = 9 oligomer clearly has two conformations at lower ($\sim 85~e$) and higher ($\sim 95~e$) charge. This trend in charging

with increasing size (shown by a gray arrow) indicates that at n = 10, only the lower charge conformer exists (shifted to slightly higher charge (~97 e) owing to the higher mass). These data indicate that a more compact conformational state is strongly favored for the n = 10 species. It is more difficult to distinguish individual peaks corresponding to different conformations in the charge plots for higher order oligomers due to the heterogeneity inherent to MDa-sized complexes and their lower overall abundance, but there is a clear overall shift of the elongated species towards forming more compact structures at larger sizes.

The same analysis was performed for the highly charged ions above the Rayleigh line (Figure 1c and Figure 3 black data). The broader range of charging shows that the higher charged species have more conformational heterogeneity than the compact forms, and that this heterogeneity increases with increasing oligomer size. There is a difference of $\sim +50$ e between the most elongated conformation of each oligomer between n = 1 and n = 5. This approximately linear increase in charge indicates that these species are highly elongated. However, beginning at n = 3, the abundance of lower charge ($\sim 71 e$ and $\sim 107 e$) peaks are indicative of the formation of more compact, partially elongated structures. These peaks may arise from the aggregation of both elongated and compact conformers or from the structural rearrangement of larger elongated species into more compact structures. Three distinct peaks are also observed for the n = 4oligomer (\sim 75 e, \sim 142 e, and \sim 189 e), which are mostly consolidated into two peaks at intermediate charges of \sim 122 e and \sim 180 e for the n=5 predominant pentameric species (Figure 3), consistent with the two less compact structures observed in the QTOF data (Figure 1a). The fully elongated species of the pentamer mAb (~240 e) appears to be heavily disfavored compared to the two more compact, but still elongated, species. These data demonstrate that small

oligomers can have considerable conformational heterogeneity and that the structures and conformational ensemble of each successive oligomer can change significantly.

For aggregates larger than the pentamer mAb, the extent of charging for the elongated forms decreases suddenly. The charge-state distribution for the n = 6 oligomer has two peaks for elongated conformations that are both $\sim 30 e$ lower charge than the two peaks for elongated species of the n = 5 oligomer. Larger aggregates show a gradual increase in the extent of charging until the n = 10 oligomer. The peaks at ~184 e and ~203 e for the n = 10 oligomer are significantly lower in abundance for the n = 11 oligomer whereas the lower charge $\sim 157 e$ peak remains abundant, indicative of a preference for a more compact structure despite the increase in mass and oligomeric state. Resolution of distinct peaks in the charge-state distribution is lost with increasing oligomer size due to the increasing inherent heterogeneity of these larger complexes. However, the overall distribution of charge states for the less compact oligomers between n = 11 and n = 15 increases at a rate similar to that of the compact forms. This suggests that the elongated forms of successively larger mAb oligomers progressively tend toward more globular structures. These data clearly show that the pentamer mAb (n = 5) and pentamer mAb dimer (n = 10) have distinct conformations that are important in the aggregation process. The oligomeric states subsequent to these key species yield ions with lower charge, suggesting more compact structures are formed via structural rearrangement. These data demonstrate that CDMS can clearly track conformational changes associated with the oligomerization processes of large proteins and also indicate that mAb oligomers possess unique conformations that are not merely amorphous aggregates of monomer subunits.

CDMS appears to be uniquely suited for characterizing the aggregation process of species with masses extending into the MDa range due to the ability to readily resolve individual

oligomers both by mass and by conformation. The ability to readily resolve many different conformers of the same mass ion based on resolved charge-state distributions irrespective of overlapping m/z values with other ions is analogous to the ability of ion mobility combined with mass spectrometry to resolve different conformers based on differences in collisional cross sections.⁵⁹ These features of CDMS show significant promise as a characterization technique to investigate antibody aggregation during the development, storage, and shipment of pharmaceuticals, as well as early stage, transient protein oligomers implicated in neurodegenerative diseases.

Conclusions

Information about the masses and conformations of large macromolecular complexes can be readily obtained using CDMS even for highly heterogeneous mixtures, making it a promising technique for studying monoclonal antibody aggregation and degradation products. Protein charge-state distributions generated from ESI reflect solution-phase conformations. The presence of multiple resolved charge-state distributions for the same size oligomer indicates that these different structures exist in solution and are preserved through the ionization process under the soft mass spectrometry interface conditions that were used. Many aggregates of a mAb and pentamer mAb complex that are detected and resolved by CDMS are not detected by other methods often used to measure the extent of aggregation. The pentamer mAb and dimers are observed with mass photometry, conventional native MS, and SEC, as are species corresponding to the mAb heavy chain, and dimer and trimer mAb complexes. In addition to these species, the CDMS data clearly shows the presence of oligomers with up to 15 mAb molecules and masses up to ~2.4 MDa. CDMS measurements enable the analysis of the charge-state distribution for

each oligomer, providing insights into the conformational heterogeneity of the oligomerization/aggregation process. In this respect, the CDMS data provide both mass and shape information comparable to that obtained by ion mobility spectrometry, but at a much larger molecular size. This type of information should prove useful for characterizing aggregation-prone proteins associated with neurodegenerative disease and for the design of drugs or buffer additives that inhibit protein aggregation because specific forms of the aggregates can be targeted and readily analyzed. Aggregates of mAb therapeutics can be formed during development, purification, formulation, and storage and may have unwanted side-effects in patients. CDMS appears to be well-suited for characterizing protein conformations and aggregation products at the level of individual oligomers that could prove beneficial at different stages of drug development, for quality control, and for optimizing formulations for biopharmaceutical stability.

Supporting Information

QTOF MS mass spectrum and CDMS 2D mass-charge histogram of a fraction collected from the predominant peak in the SEC trace.

Author Information

There are no conflicts of interest to declare.

Acknowledgements

This material is based upon work supported by the National Science Foundation Division of Chemistry under grant number CHE-2203907, an ACS Graduate Research Fellowship sponsored by Eli Lilly and Company (J.S.J.), the Arnold and Mabel Beckman Foundation Postdoctoral

Fellowship in Chemical Instrumentation (C.C.H.), Merck & Co., Inc., San Francisco, CA, USA, Inc. through their Discovery Biologics SEEDS program, and the National Institutes of Health (grant 5R01GM139338) for the development and construction of the charge detection mass spectrometer used in this research.

References

- (1) Ross, C. A.; Poirier, M. A. Protein Aggregation and Neurodegenerative Disease. *Nat. Med.* **2004**, *10* (S7), S10–S17. https://doi.org/10.1038/nm1066.
- (2) Stefani, M.; Dobson, C. M. Protein Aggregation and Aggregate Toxicity: New Insights into Protein Folding, Misfolding Diseases and Biological Evolution. *J. Mol. Med.* **2003**, 81 (11), 678–699. https://doi.org/10.1007/s00109-003-0464-5.
- (3) Ratanji, K. D.; Derrick, J. P.; Dearman, R. J.; Kimber, I. Immunogenicity of Therapeutic Proteins: Influence of Aggregation. *J. Immunotoxicol.* **2014**, *11* (2), 99–109. https://doi.org/10.3109/1547691X.2013.821564.
- (4) Swanson, M. D.; Rios, S.; Mittal, S.; Soder, G.; Jawa, V. Immunogenicity Risk Assessment of Spontaneously Occurring Therapeutic Monoclonal Antibody Aggregates. *Front. Immunol.* **2022**, *13* (July), 1–11. https://doi.org/10.3389/fimmu.2022.915412.
- (5) Wang, W.; Singh, S. K.; Li, N.; Toler, M. R.; King, K. R.; Nema, S. Immunogenicity of Protein Aggregates—Concerns and Realities. *Int. J. Pharm.* **2012**, *431* (1–2), 1–11. https://doi.org/10.1016/j.ijpharm.2012.04.040.
- (6) United States Food and Drug Administration. *Guidance for Industry Q6B Specifications:* Test Procedures and Acceptance Criteria for Biotechnological/Biological Products; 1999.
- (7) den Engelsman, J.; Garidel, P.; Smulders, R.; Koll, H.; Smith, B.; Bassarab, S.; Seidl, A.; Hainzl, O.; Jiskoot, W. Strategies for the Assessment of Protein Aggregates in Pharmaceutical Biotech Product Development. *Pharm. Res.* **2011**, *28* (4), 920–933. https://doi.org/10.1007/s11095-010-0297-1.
- (8) Rosati, S.; Yang, Y.; Barendregt, A.; Heck, A. J. R. Detailed Mass Analysis of Structural Heterogeneity in Monoclonal Antibodies Using Native Mass Spectrometry. *Nat. Protoc.* **2014**, *9* (4), 967–976. https://doi.org/10.1038/nprot.2014.057.
- (9) Villafuerte-Vega, R. C.; Li, H. W.; Slaney, T. R.; Chennamsetty, N.; Chen, G.; Tao, L.; Ruotolo, B. T. Ion Mobility-Mass Spectrometry and Collision-Induced Unfolding of Designed Bispecific Antibody Therapeutics. *Anal. Chem.* **2023**, *95* (17), 6962–6970. https://doi.org/10.1021/acs.analchem.3c00344.
- (10) Campuzano, I. D. G.; Netirojjanakul, C.; Nshanian, M.; Lippens, J. L.; Kilgour, D. P. A.; Van Orden, S.; Loo, J. A. Native-MS Analysis of Monoclonal Antibody Conjugates by Fourier Transform Ion Cyclotron Resonance Mass Spectrometry. *Anal. Chem.* **2018**, *90* (1), 745–751. https://doi.org/10.1021/acs.analchem.7b03021.
- (11) Tamara, S.; den Boer, M. A.; Heck, A. J. R. High-Resolution Native Mass Spectrometry. *Chem. Rev.* **2022**, *122* (8), 7269–7326. https://doi.org/10.1021/acs.chemrev.1c00212.

- (12) Susa, A. C.; Xia, Z.; Williams, E. R. Native Mass Spectrometry from Common Buffers with Salts That Mimic the Extracellular Environment. *Angew. Chem. Int. Ed.* **2017**, *56* (27), 7912–7915. https://doi.org/10.1002/anie.201702330.
- (13) Susa, A. C.; Xia, Z.; Williams, E. R. Small Emitter Tips for Native Mass Spectrometry of Proteins and Protein Complexes from Nonvolatile Buffers That Mimic the Intracellular Environment. *Anal. Chem.* **2017**, *89* (5), 3116–3122. https://doi.org/10.1021/acs.analchem.6b04897.
- (14) Harper, C. C.; Miller, Z. M.; Lee, H.; Bischoff, A. J.; Francis, M. B.; Schaffer, D. V.; Williams, E. R. Effects of Molecular Size on Resolution in Charge Detection Mass Spectrometry. *Anal. Chem.* **2022**, *94* (33), 11703–11712. https://doi.org/10.1021/acs.analchem.2c02572.
- (15) Grande, A. E.; Li, X.; Miller, L. M.; Zhang, J.; Draper, B. E.; Herzog, R. W.; Xiao, W.; Jarrold, M. F. Antibody Binding to Recombinant Adeno Associated Virus Monitored by Charge Detection Mass Spectrometry. *Anal. Chem.* **2023**, *95* (29), 10864–10868. https://doi.org/10.1021/acs.analchem.3c02371.
- (16) Barnes, L. F.; Draper, B. E.; Jarrold, M. F. Analysis of Recombinant Adenovirus Vectors by Ion Trap Charge Detection Mass Spectrometry: Accurate Molecular Weight Measurements beyond 150 MDa. *Anal. Chem.* **2022**, *94* (3), 1543–1551. https://doi.org/10.1021/acs.analchem.1c02439.
- (17) Barnes, L. F.; Draper, B. E.; Kurian, J.; Chen, Y. T.; Shapkina, T.; Powers, T. W.; Jarrold, M. F. Analysis of AAV-Extracted DNA by Charge Detection Mass Spectrometry Reveals Genome Truncations. *Anal. Chem.* **2023**, *95* (9), 4310–4316. https://doi.org/10.1021/acs.analchem.2c04234.
- (18) Bischoff, A. J.; Harper, C. C.; Williams, E. R.; Francis, M. B. Characterizing Heterogeneous Mixtures of Assembled States of the Tobacco Mosaic Virus Using Charge Detection Mass Spectrometry. *J. Am. Chem. Soc.* **2022**, *144* (51), 23368–23378. https://doi.org/10.1021/jacs.2c09160.
- (19) Miller, Z. M.; Harper, C. C.; Lee, H.; Bischoff, A. J.; Francis, M. B.; Schaffer, D. V.; Williams, E. R. Apodization Specific Fitting for Improved Resolution, Charge Measurement, and Data Analysis Speed in Charge Detection Mass Spectrometry. *J. Am. Soc. Mass Spectrom.* **2022**, *33* (11), 2129–2137. https://doi.org/10.1021/jasms.2c00213.
- (20) Miller, L. M.; Bond, K. M.; Draper, B. E.; Jarrold, M. F. Characterization of Classical Vaccines by Charge Detection Mass Spectrometry. *Anal. Chem.* **2021**, *93* (35), 11965–11972. https://doi.org/10.1021/acs.analchem.1c01893.
- (21) Harper, C. C.; Avadhani, V. S.; Hanozin, E.; Miller, Z. M.; Williams, E. R. Dynamic Energy Measurements in Charge Detection Mass Spectrometry Eliminate Adverse Effects of Ion–Ion Interactions. *Anal. Chem.* **2023**, *95* (26), 10077–10086. https://doi.org/10.1021/acs.analchem.3c01520.
- (22) Harper, C. C.; Elliott, A. G.; Oltrogge, L. M.; Savage, D. F.; Williams, E. R. Multiplexed Charge Detection Mass Spectrometry for High-Throughput Single Ion Analysis of Large Molecules. *Anal. Chem.* **2019**, *91* (11), 7458–7465. https://doi.org/10.1021/acs.analchem.9b01669.
- (23) Harper, C. C.; Williams, E. R. Enhanced Multiplexing in Fourier Transform Charge Detection Mass Spectrometry by Decoupling Ion Frequency from Mass to Charge Ratio. *J. Am. Soc. Mass Spectrom.* **2019**, *30* (12), 2637–2645. https://doi.org/10.1007/s13361-019-02330-3.

- (24) El-Baba, T. J.; Raab, S. A.; Buckley, R. P.; Brown, C. J.; Lutomski, C. A.; Henderson, L. W.; Woodall, D. W.; Shen, J.; Trinidad, J. C.; Niu, H.; Jarrold, M. F.; Russell, D. H.; Laganowsky, A.; Clemmer, D. E. Thermal Analysis of a Mixture of Ribosomal Proteins by vT-ESI-MS: Toward a Parallel Approach for Characterizing the *Stabilitome. Anal. Chem.* **2021**, *93* (24), 8484–8492. https://doi.org/10.1021/acs.analchem.1c00772.
- (25) Anthony, A. J.; Gautam, A. K. S.; Miller, L. M.; Ma, Y.; Hardwick, A. G.; Sharma, A.; Ghatak, S.; Matouschek, A.; Jarrold, M. F.; Clemmer, D. E. CDMS Analysis of Intact 19S, 20S, 26S, and 30S Proteasomes: Evidence for Higher-Order 20S Assemblies at a Low pH. *Anal. Chem.* **2023**, *95* (33), 12209–12215. https://doi.org/10.1021/acs.analchem.3c00472.
- (26) Elliott, A. G.; Harper, C. C.; Lin, H.-W.; Williams, E. R. Effects of Individual Ion Energies on Charge Measurements in Fourier Transform Charge Detection Mass Spectrometry (FT-CDMS). *J. Am. Soc. Mass Spectrom.* **2019**, *30* (6), 946–955. https://doi.org/10.1007/s13361-018-2094-8.
- (27) Elliott, A. G.; Harper, C. C.; Lin, H. W.; Williams, E. R. Mass, Mobility and MSⁿ Measurements of Single Ions Using Charge Detection Mass Spectrometry. *Analyst* **2017**, *142* (15), 2760–2769. https://doi.org/10.1039/C7AN00618G.
- (28) Harper, C. C.; Elliott, A. G.; Lin, H. W.; Williams, E. R. Determining Energies and Cross Sections of Individual Ions Using Higher-Order Harmonics in Fourier Transform Charge Detection Mass Spectrometry (FT-CDMS). *J. Am. Soc. Mass Spectrom.* **2018**, *29* (9), 1861–1869. https://doi.org/10.1007/s13361-018-1987-x.
- (29) Halim, M. A.; Clavier, C.; Dagany, X.; Kerleroux, M.; Dugourd, P.; Dunbar, R. C.; Antoine, R. Infrared Laser Dissociation of Single Megadalton Polymer Ions in a Gated Electrostatic Ion Trap: The Added Value of Statistical Analysis of Individual Events. *Phys. Chem. Chem. Phys.* **2018**, *20* (17), 11959–11966. https://doi.org/10.1039/C8CP00404H.
- (30) McPartlan, M. S.; Harper, C. C.; Hanozin, E.; Williams, E. R. Ion Emission from 1–10 MDa Salt Clusters: Individual Charge State Resolution with Charge Detection Mass Spectrometry. *Analyst* **2024**, *149* (3), 735-744. https://doi.org/10.1039/D3AN01913F.
- (31) Hanozin, E.; Harper, C. C.; McPartlan, M. S.; Williams, E. R. Dynamics of Rayleigh Fission Processes in ~100 nm Charged Aqueous Nanodrops. *ACS Cent. Sci.* **2023**, *9* (8), 1611–1622. https://doi.org/10.1021/acscentsci.3c00323.
- (32) Harper, C. C.; Brauer, D. D.; Francis, M. B.; Williams, E. R. Direct Observation of Ion Emission from Charged Aqueous Nanodrops: Effects on Gaseous Macromolecular Charging. *Chem. Sci.* **2021**, *12* (14), 5185–5195. https://doi.org/10.1039/D0SC05707J.
- (33) Harper, C. C.; Miller, Z. M.; McPartlan, M. S.; Jordan, J. S.; Pedder, R. E.; Williams, E. R. Accurate Sizing of Nanoparticles Using a High-Throughput Charge Detection Mass Spectrometer without Energy Selection. *ACS Nano* **2023**, *17* (8), 7765–7774. https://doi.org/10.1021/acsnano.3c00539.
- (34) Doussineau, T.; Bao, C. Y.; Antoine, R.; Dugourd, P.; Zhang, W.; D'Agosto, F.; Charleux, B. Direct Molar Mass Determination of Self-Assembled Amphiphilic Block Copolymer Nanoobjects Using Electrospray-Charge Detection Mass Spectrometry. *ACS Macro Lett.* **2012**, *1* (3), 414–417. https://doi.org/10.1021/mz300011b.
- (35) Doussineau, T.; Désert, A.; Lambert, O.; Taveau, J. C.; Lansalot, M.; Dugourd, P.; Bourgeat-Lami, E.; Ravaine, S.; Duguet, E.; Antoine, R. Charge Detection Mass Spectrometry for the Characterization of Mass and Surface Area of Composite Nanoparticles. *J. Phys. Chem. C* **2015**, *119* (20), 10844–10849. https://doi.org/10.1021/jp510081v.

- (36) Kostelic, M. M.; Ryan, J. P.; Brown, L. S.; Jackson, T. W.; Hsieh, C.; Zak, C. K.; Sanders, H. M.; Liu, Y.; Chen, V. S.; Byrne, M.; Aspinwall, C. A.; Baker, E. S.; Marty, M. T. Stability and Dissociation of Adeno-Associated Viral Capsids by Variable Temperature-Charge Detection-Mass Spectrometry. *Anal. Chem.* **2022**, *94* (34), 11723–11727. https://doi.org/10.1021/acs.analchem.2c02378.
- (37) Lai, S. H.; Tamara, S.; Heck, A. J. R. Single-Particle Mass Analysis of Intact Ribosomes by Mass Photometry and Orbitrap-Based Charge Detection Mass Spectrometry. *iScience* **2021**, *24* (11), 103211. https://doi.org/10.1016/j.isci.2021.103211.
- (38) Kafader, J. O.; Melani, R. D.; Durbin, K. R.; Ikwuagwu, B.; Early, B. P.; Fellers, R. T.; Beu, S. C.; Zabrouskov, V.; Makarov, A. A.; Maze, J. T.; Shinholt, D. L.; Yip, P. F.; Tullman-Ercek, D.; Senko, M. W.; Compton, P. D.; Kelleher, N. L. Multiplexed Mass Spectrometry of Individual Ions Improves Measurement of Proteoforms and Their Complexes. *Nat. Methods* 2020, *17* (4), 391–394. https://doi.org/10.1038/s41592-020-0764-5.
- (39) McGee, J. P.; Melani, R. D.; Yip, P. F.; Senko, M. W.; Compton, P. D.; Kafader, J. O.; Kelleher, N. L. Isotopic Resolution of Protein Complexes up to 466 KDa Using Individual Ion Mass Spectrometry. *Anal. Chem.* **2021**, *93* (5), 2723–2727. https://doi.org/10.1021/acs.analchem.0c03282.
- (40) den Boer, M. A.; Lai, S. H.; Xue, X.; van Kampen, M. D.; Bleijlevens, B.; Heck, A. J. R. Comparative Analysis of Antibodies and Heavily Glycosylated Macromolecular Immune Complexes by Size-Exclusion Chromatography Multi-Angle Light Scattering, Native Charge Detection Mass Spectrometry, and Mass Photometry. *Anal. Chem.* 2022, 94 (2), 892–900. https://doi.org/10.1021/acs.analchem.1c03656.
- (41) Du, C.; Cleary, S. P.; Kostelic, M. M.; Jones, B. J.; Kafader, J. O.; Wysocki, V. H. Combining Surface-Induced Dissociation and Charge Detection Mass Spectrometry to Reveal the Native Topology of Heterogeneous Protein Complexes. *Anal. Chem.* **2023**, *95* (37), 13889–13896. https://doi.org/10.1021/acs.analchem.3c02185.
- (42) Hundt, N.; Cole, D.; Hantke, M. F.; Miller, J. J.; Struwe, W. B.; Kukura, P. Direct Observation of the Molecular Mechanism Underlying Protein Polymerization. *Sci. Adv.* **2022**, *8* (35), eabm7935. https://doi.org/10.1126/sciadv.abm7935.
- (43) Young, G.; Hundt, N.; Cole, D.; Fineberg, A.; Andrecka, J.; Tyler, A.; Olerinyova, A.; Ansari, A.; Marklund, E. G.; Collier, M. P.; Chandler, S. A.; Tkachenko, O.; Allen, J.; Crispin, M.; Billington, N.; Takagi, Y.; Sellers, J. R.; Eichmann, C.; Selenko, P.; Frey, L.; Riek, R.; Galpin, M. R.; Struwe, W. B.; Benesch, J. L. P.; Kukura, P. Quantitative Mass Imaging of Single Biological Macromolecules. *Science*, **2018**, *360* (6387), 423–427. https://doi.org/10.1126/science.aar5839.
- (44) Liebthal, M.; Kushwah, M. S.; Kukura, P.; Dietz, K. J. Single Molecule Mass Photometry Reveals the Dynamic Oligomerization of Human and Plant Peroxiredoxins. *iScience* **2021**, 24 (11), 103258. https://doi.org/10.1016/j.isci.2021.103258.
- (45) Lai, S. H.; Reynaud, A.; Zhang, N. N.; Kwak, M.; Vysotskyi, B.; Dominguez-Medina, S.; Fortin, T.; Clement, K.; Defoort, M.; Lee, T. G.; Liu, K.; Hentz, S.; Masselon, C. D. Characterizing Nanoparticle Mass Distributions Using Charge-Independent Nanoresonator Mass Spectrometry. *J. Phys. Chem. C* 2022, *126* (49), 20946–20953. https://doi.org/10.1021/acs.jpcc.2c06675.
- (46) Dominguez-Medina, S.; Fostner, S.; Defoort, M.; Sansa, M.; Stark, A. K.; Halim, M. A.; Vernhes, E.; Gely, M.; Jourdan, G.; Alava, T.; Boulanger, P.; Masselon, C.; Hentz, S.

- Neutral Mass Spectrometry of Virus Capsids above 100 Megadaltons with Nanomechanical Resonators. *Science* **2018**, *362* (6417), 918–922. https://doi.org/10.1126/science.aat6457.
- (47) Kaynak, B. E.; Alkhaled, M.; Kartal, E.; Yanik, C.; Hanay, M. S. Atmospheric-Pressure Mass Spectrometry by Single-Mode Nanoelectromechanical Systems. *Nano Lett.* **2023**, *23* (18), 8553–8559. https://doi.org/10.1021/acs.nanolett.3c02343.
- (48) Wörner, T. P.; Thurman, H. A.; Makarov, A. A.; Shvartsburg, A. A. Expanding Differential Ion Mobility Separations into the MegaDalton Range. *Anal. Chem.* **2024**. https://doi.org/10.1021/acs.analchem.3c05012.
- (49) Jordan, J. S.; Xia, Z.; Williams, E. R. Tips on Making Tiny Tips: Secrets to Submicron Nanoelectrospray Emitters. *J. Am. Soc. Mass Spectrom.* **2022**, *33* (3), 607–611. https://doi.org/10.1021/jasms.1c00372.
- (50) Harper, C. C.; Miller, Z. M.; Williams, E. R. Combined Multiharmonic Frequency Analysis for Improved Dynamic Energy Measurements and Accuracy in Charge Detection Mass Spectrometry. *Anal. Chem.* **2023**, *95* (45), 16659–16667. https://doi.org/10.1021/acs.analchem.3c03160.
- (51) Chowdhury, S. K.; Katta, V.; Chait, B. T. Probing Conformation Changes in Proteins by Mass Spectrometry. *J. Am. Chem. Soc.* **1990**, *112* (24), 9012–9013. https://doi.org/10.1021/ja00180a074.
- (52) Cassou, C. A.; Williams, E. R. Desalting Protein Ions in Native Mass Spectrometry Using Supercharging Reagents. *Analyst* **2014**, *139* (19), 4810–4819. https://doi.org/10.1039/C4AN01085J.
- (53) Iavarone, A. T.; Udekwu, O. A.; Williams, E. R. Buffer Loading for Counteracting Metal Salt-Induced Signal Suppression in Electrospray Ionization. *Anal. Chem.* 2004, 76 (14), 3944–3950. https://doi.org/10.1021/ac049724+.
- (54) Flick, T. G.; Merenbloom, S. I.; Williams, E. R. Anion Effects on Sodium Ion and Acid Molecule Adduction to Protein Ions in Electrospray Ionization Mass Spectrometry. *J. Am. Soc. Mass Spectrom.* **2011**, *22* (11), 1968-1977. https://doi.org/10.1007/s13361-011-0218-5.
- (55) Jordan, J. S.; Williams, E. R. Effects of Electrospray Droplet Size on Analyte Aggregation: Evidence for Serine Octamer in Solution. *Anal. Chem.* **2021**, *93* (3), 1725–1731. https://doi.org/10.1021/acs.analchem.0c04343.
- (56) Jordan, J. S.; Williams, E. R. Homochiral Preference of Serine Octamer in Solution and Formed by Dissociation of Large Gaseous Clusters. *Analyst* **2021**, *146* (22), 6822–6830. https://doi.org/10.1039/d1an01646f.
- (57) Davidson, K. L.; Oberreit, D. R.; Hogan, C. J.; Bush, M. F. Nonspecific Aggregation in Native Electrokinetic Nanoelectrospray Ionization. *Int. J. Mass Spectrom.* **2017**, *420*, 35–42. https://doi.org/10.1016/j.ijms.2016.09.013.
- (58) Wiesner, R.; Scheller, C.; Krebs, F.; Wätzig, H.; Oltmann-Norden, I. A Comparative Study of CE-SDS, SDS-PAGE, and Simple Western: Influences of Sample Preparation on Molecular Weight Determination of Proteins. *Electrophoresis* **2021**, *42* (3), 206–218. https://doi.org/10.1002/elps.202000199.
- (59) Bleiholder, C.; Bowers, M. T. The Solution Assembly of Biological Molecules Using Ion Mobility Methods: From Amino Acids to Amyloid β-Protein. *Annu. Rev. Anal. Chem.* 2017, 10 (1), 365–386. https://doi.org/10.1146/annurev-anchem-071114-040304.

(60) Mortensen, D. N.; Williams, E. R. Ultrafast (1 μs) Mixing and Fast Protein Folding in Nanodrops Monitored by Mass Spectrometry. *J. Am. Chem. Soc.* **2016**, *138*, 3453-3460. https://doi.org/10.1021/jacs.5b13081

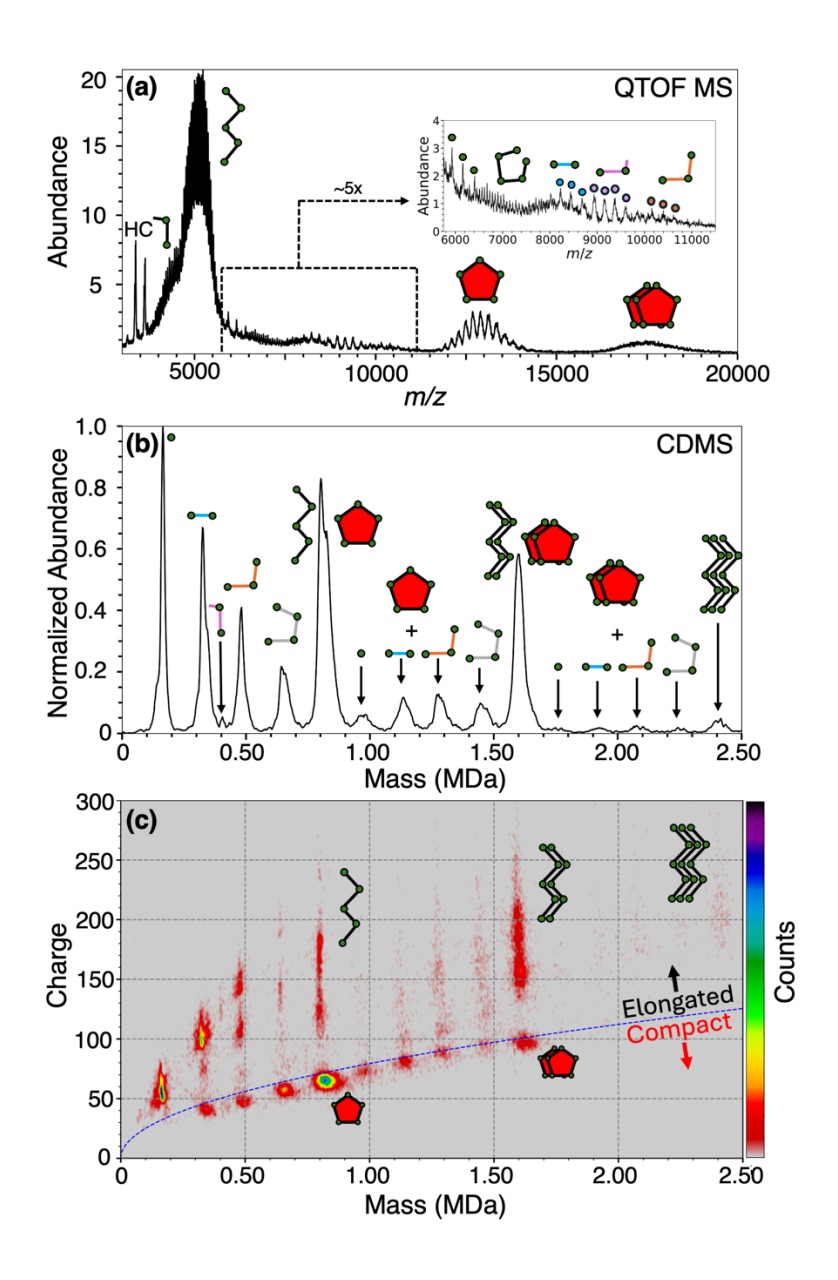


Figure 1. Mass spectral data from a pentameric mAb sample acquired using (a) native mass spectrometry with a QTOF mass spectrometer and (b,c) charge detection mass spectrometry using a custom built instrument. The inset in (a) is an expansion of the region from m/z 5,500 – 12,000 and shows the overlapping charge-state distributions in this region that indicate the presence of unresolved species. The CDMS 1D mass histogram in (b) is analogous to a deconvolved mass spectrum obtained by conventional native MS, whereas the CDMS 2D histogram in (c) disperses ion signal based on mass (x-axis) and charge (y-axis) with abundance

indicated by the color code to the right of the plot. The blue dashed line in (c) corresponds to the Rayleigh limit for an aqueous droplet as a function of mass. Distributions above the Rayleigh line in (c) correspond to ions with an elongated conformation, whereas ions below this line have more compact structures that are more spherical.

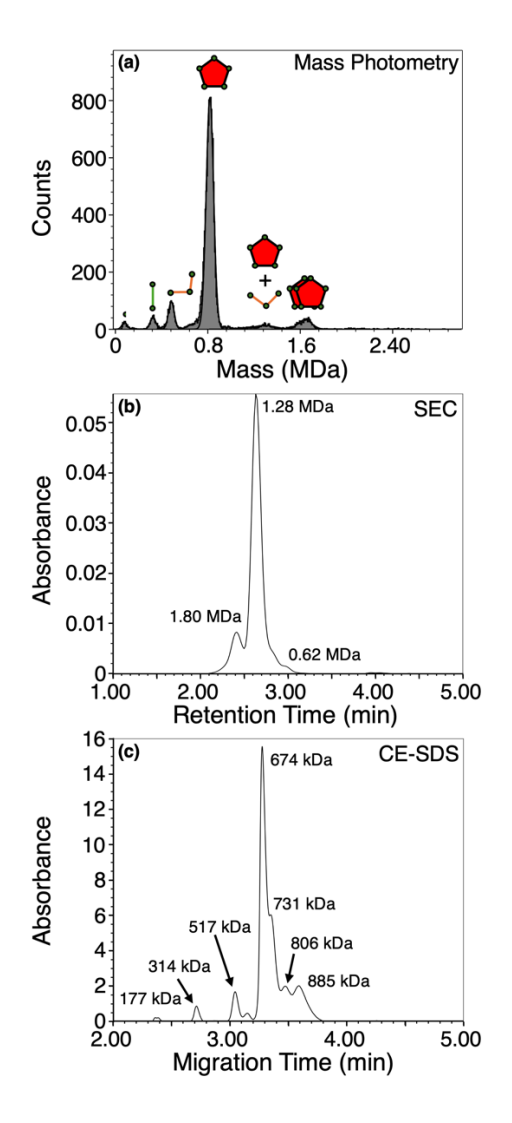


Figure 2. (a) Mass photometry histogram, (b) a SEC trace, and (c) a CE-SDS trace of the same pentameric mAb sample. Mass photometry signal for the pentamer mAb monomer and dimer is observed along with smaller species corresponding to a mAb heavy chain, as well as a mAb dimer and trimer. The molecular weights assigned to peaks in the SEC and CE-SDS traces in (b) and (c) were calculated based on the retention time or migration time of molecular weight standards with masses between 112 Da and 1.3 MDa. These masses and abundances do not directly correspond to species observed in the QTOF, CDMS, or mass photometry data, making assignments of these peaks ambiguous.

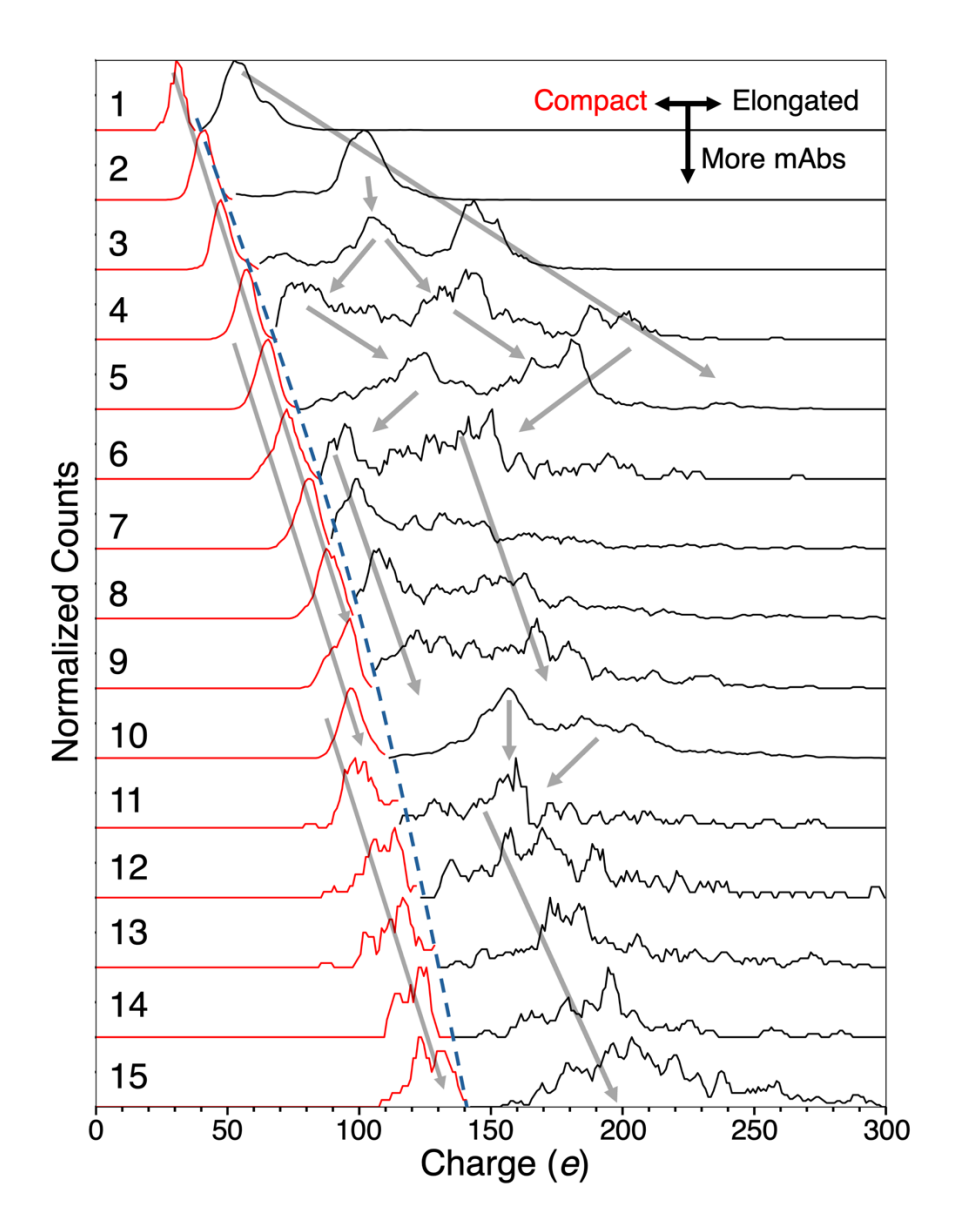


Figure 3. CDMS data shown in Figure 1c is replotted as a function of charge (*x*-axis) vs. the normalized abundances of each observed oligomeric species (*y*-axis) and shows the evolution of the structures of compact forms of the oligomers (charged near or below the Rayleigh limit; data in red) and the more elongated forms of the oligomers (charges above the Rayleigh limit; data in black). The numbers progressing down the *y*-axis correspond to the increasing number of mAb molecules in each oligomer. Data to the left and right of the blue dashed line are normalized

separately so that the compact and elongated conformers can more clearly be compared on the same figure. Arrows show trends in conformational heterogeneity as a function of oligomer size.

TOC Figure

